Theoretical and Applied Fracture Mechanics 128 (2023) 104105

Contents lists available at ScienceDirect

Theoretical and Applied Fracture Mechanics

journal homepage: www.elsevier.com/locate/tafmec

Discontinuous quarter-point boundary elements revisited: Computation of T-stress in two-dimensional cracked components

C. Baena [a], F. García-Sánchez [b,*], A. Sáez [c]

[a] Escuela Técnica Superior de Ingeniería Informática, Universidad de Sevilla, Av. Reina Mercedes s/n, 41012 Sevilla, Spain
[b] Escuela de Ingenierías Industriales, Universidad de Málaga, Calle Dr. Ortiz Ramos s/n, 29071 Málaga, Spain
[c] Escuela Técnica Superior de Ingeniería, Universidad de Sevilla, Camino de los Descubrimientos s/n, 41092 Sevilla, Spain

ARTICLE INFO

Keywords:
T-stress
Stress intensity factors
Dual Boundary Element Method (BEM)
Fracture mechanics
Discontinuous quarter-point element

ABSTRACT

This paper analyzes the use of discontinuous quarter-point quadratic elements in a dual or hypersingular boundary element context to compute the T-stress for cracked 2-D isotropic components. The performance of this approach has been demonstrated in the past for stress intensity factors (SIFs) computation and, herein, it is revisited to assess its adequacy for T-stress evaluation. To this end, novel direct extrapolation formulas that determine the T-stress from the computed nodal displacements at the collocation nodes of the discontinuous quarter-point element are proposed, and their accuracy and effectiveness is satisfactorily tested by several numerical examples involving 2-D cracked Carbon NanoTube (CNT) reinforced composites. SIFs extrapolated from the computed nodal crack opening displacements and T-stress evaluated from the computed stresses at internal points (close to the crack-tip) are also presented for completeness. The proposed techniques are a valid and easy-to-implement alternative to the interaction integral approaches when determining SIFs and T-stress.

1. Introduction

In modern engineering, reliable numerical tools able to simulate the behavior of cracked domains, when subjected to any general loading condition, play a critical role in life assessment of structural components. These tools must be able to simulate the singular behavior occurring around the crack-tip and further provide the relevant fracture parameters in an accurate and straightforward manner.

In the case of isotropic linear elastic materials, fracture behavior is characterized by the well-known Williams' series expansion, which for plane problems describes the asymptotic stress field around the crack-tip as [1,2]

$$\sigma_{11}(r,\theta) = \frac{K_I}{\sqrt{2\pi r}} cos\frac{\theta}{2}\left(1 - sin\frac{\theta}{2}sin\frac{3\theta}{2}\right) - \frac{K_{II}}{\sqrt{2\pi r}} sin\frac{\theta}{2}\left(2 + cos\frac{\theta}{2}cos\frac{3\theta}{2}\right) + T + O(r^{1/2}) \tag{1}$$

$$\sigma_{22}(r,\theta) = \frac{K_I}{\sqrt{2\pi r}} cos\frac{\theta}{2}\left(1 + sin\frac{\theta}{2}sin\frac{3\theta}{2}\right) + \frac{K_{II}}{\sqrt{2\pi r}} sin\frac{\theta}{2}cos\frac{\theta}{2}cos\frac{3\theta}{2} + O(r^{1/2}) \tag{2}$$

$$\sigma_{12}(r,\theta) = \frac{K_I}{\sqrt{2\pi r}} cos\frac{\theta}{2}sin\frac{\theta}{2}cos\frac{3\theta}{2} + \frac{K_{II}}{\sqrt{2\pi r}} cos\frac{\theta}{2}\left(1 - sin\frac{\theta}{2}sin\frac{3\theta}{2}\right) + O(r^{1/2}) \tag{3}$$

and the displacement field in the vicinity of the crack-tip as

$$u_1(r,\theta) = u_{10} + \frac{K_I}{2\mu}\sqrt{\frac{r}{2\pi}}\left[\left(\kappa - \frac{1}{2}\right)cos\frac{\theta}{2} - \frac{1}{2}cos\frac{3\theta}{2}\right] + \frac{K_{II}}{2\mu}\sqrt{\frac{r}{2\pi}}\left[\left(\kappa + \frac{3}{2}\right)sin\frac{\theta}{2} + \frac{1}{2}sin\frac{3\theta}{2}\right] + \frac{T}{4}\frac{r}{2\mu}(\kappa + 1)cos\theta + O(r^{3/2}) \tag{4}$$

$$u_2(r,\theta) = u_{20} + \frac{K_I}{2\mu}\sqrt{\frac{r}{2\pi}}\left[\left(\kappa + \frac{1}{2}\right)sin\frac{\theta}{2} - \frac{1}{2}sin\frac{3\theta}{2}\right] - \frac{K_{II}}{2\mu}\sqrt{\frac{r}{2\pi}}\left[\left(\kappa - \frac{3}{2}\right)cos\frac{\theta}{2} + \frac{1}{2}cos\frac{3\theta}{2}\right] + \frac{T}{4}\frac{r}{2\mu}(\kappa - 3)sin\theta + O(r^{3/2}) \tag{5}$$

* Corresponding author.
E-mail addresses: cbaena@us.es (C. Baena), fgsanchez@uma.es (F. García-Sánchez), andres@us.es (A. Sáez).

https://doi.org/10.1016/j.tafmec.2023.104105
Received 15 April 2023; Received in revised form 7 August 2023; Accepted 25 September 2023
Available online 30 September 2023

where (r,θ) are cylindrical coordinates centered at the crack tip (Fig. 1.a); K_I and K_{II} stand for the mode-I and mode-II Stress Intensity Factors (SIFs), respectively; T denotes the T-stress; μ is the shear modulus and ν is the Poisson's ratio, so that the Young's modulus is given by $E = 2\mu(1+\nu)$; and κ is the Kolosov's constant, defined as $\kappa = 3-4\nu$ for plane strain or $\kappa = (3-\nu)/(1+\nu)$ for plane stress. u_{10} and u_{20} are the displacements at the crack tip and, as expected, do no contribute to neither the stresses nor the strains.

In Eqs. (1)–(3), the SIFs correspond to the singular terms of Williams' series expansion for the stress field, while the leading non-singular term, which corresponds to a constant stress acting parallel to the crack plane, is the so-called T-stress. Classical fracture theories habitually neglect all but the singular terms, thus resulting into a single parameter description of the near-tip stress fields in terms of the SIFs. However, several studies reveal the importance of the T-stress in the characterization of crack stability and kinking for linear elastic materials. Furthermore, T-stress has a significant effect on the plastic zone size and shape and the tensile stress triaxiality of elastic–plastic crack-tip fields, so that it plays as well an important role in elastic–plastic fracture analysis (even though the T-stress is calculated from the linear elastic material properties). As a consequence, various fracture theories suggest the inclusion of the T-stress as a second crack-tip parameter [3–8].

Several numerical techniques have been developed to evaluate the relevant fracture parameters: SIFs and, in particular, T-stress. For instance, within the framework of the Finite Element Method (FEM), Kfouri [9] implemented path-independent contour integrals to compute the T-stress. Ayatollahi et al. [10] proposed the direct evaluation of the T-stress from the computed displacement and stress values obtained from FE analysis using rather fine meshes, while mesh-dependence of this procedure was later discussed in [11]. Chen et al. [12] combined the use of path independent integrals with a hierarchical p-version of the FEM. Karihaloo and coworkers [2] developed a hybrid crack element (HCE) with p-adaptivity and also illustrated the need for finer meshes in order to evaluate T-stress, in comparison with the ones required to accurately determine the SIFs. They later extended this procedure to mixed mode cracks [13] and further coupled their HCE with the eXtended FEM (XFEM) [14]. Su and coworkers [15,16] implemented the fractal FEM to obtain SIFs and T-stress directly from the computed coefficients using rather coarse meshes. Ayatollahi and Nejati [17] proposed an over-deterministic approach, based on the formulation of linear least-squares, to evaluate the higher-order terms in Williams' expansion using the displacement fields obtained from conventional FE analysis. More recently, Sladek et al. [18] derived simple extrapolation formulas to compute the T-stress in functionally graded materials by comparing the variation of displacements in quarter-point crack-tip elements with the corresponding asymptotic expression for the displacement field around the crack-tip. Hou and coworkers combined the interaction integral method with the XFEM to evaluate SIFs and T-stress at a central cracked Brazilian disks subjected to both confining pressure and diametric forces [19] and later proposed an over-deterministic method based on crack-tip stress fields to this end [20]. Li and Zheng [21] implemented an over-deterministic displacement field fitting method in conjunction with XFEM to evaluate these fracture parameters.

Other numerical techniques have been successfully applied as well to compute T-stress. For example, Song [22] and Chidgzey and Deeks [23] used the Scaled Boundary Finite Element Method (SBFEM) to directly evaluate the coefficients of the Williams' expansion of the linear elastic crack tip asymptotic field. This method was later extended to dynamics by Song and Vrcelj [24]. The interested reader is referred to a recent review paper by Song et al. on the application of the SBFEM to fracture analysis [25]. Meanwhile, Huang et al. [26] implemented the finite block method to evaluate both SIFs and T-stress, whilst Zhang et al. [27] employed the numerical manifold method to this end.

When it comes to solving linear elastic fracture mechanics problems, it is well established that the Boundary Element Method (BEM) is a quite efficient numerical technique [28,29]. Although seminal works determined the T-term using path-independent integrals with a rather large uncertainty [30], subsequent contributions led to more accurate T-stress estimations. Sladek et al. [31] derived contour integrals based on Betti's theorem to compute T-stress in both statics and dynamics. Yang and Ravi-Chandar [32] implemented an iterative single-domain dual BEM, together with a tip-node rule imposing zero displacement jump at the crack tip, to compute the T-term from the stresses evaluated at interior points close to the crack-tip. Tan and coworkers derived a formula to directly evaluate the elastic T-stress by adjusting the variation of the displacements along the quarter-point crack-tip element to Williams' asymptotic displacement expansion using the classical BEM formulation [33] and later implemented the M-contour integral approach to this same end [34]. In both cases, quadratic displacement and traction-singular quarter-point continuous crack-tip elements were used, so that, when meshing, the domain had to be divided in subdomains connected at interfaces where the crack is located. Sutradhar and Paulino [35] implemented the symmetric Galerkin BEM in conjunction with an interaction integral method for evaluating T-stress in mixed-mode crack problems. Phan [36] developed a non-singular boundary integral equation, based upon the asymptotic Williams' series for the stress field near the crack tip, that permitted to numerically evaluate the T-stress in the post-processing stage of any BEM crack analysis. More recently, Chen et al. [37] presented a spline fictitious boundary element alternating method to compute T-stress in multi-cracked 2-D domains, whilst Feng et al. [38] developed a dual BEM formulation to evaluate SIFs and T-stress. These latter authors claim that extrapolation methods are imprecise to compute fracture parameters and circumvent such issue by using the interaction integral approach. Although our work and this literature review mainly focuses on 2-D applications, it is worth mentioning here the recent papers by Sladek and coworkers [39,40], where the authors apply the BEM to compute static and dynamic SIFs and elasticity T-stresses in 3D cracked domains.

Many of the approaches above make use of the interaction integral method to numerically compute the fracture parameters. A recent paper by Yu and Kuna [41] presents a critical overview on the topic. At any event, direct extrapolation formulas that compute these parameters from the nodal values are straightforward and easy to implement, do not require elaborated postprocessing techniques and have proven efficient in the past, thus providing a valuable cross-check. In this regard, Sáez et al. [42] developed a dual BEM formulation that, in conjunction with the use of discontinuous quarter-point elements, allowed the precise evaluation of SIFs in isotropic materials from the computed nodal displacements. This approach is quite straightforward, robust and easy to implement and provides stable results for even rather coarse meshes. For this reasons, it was later extended successfully to static and dynamic crack analysis of anisotropic, piezoelectric or magnetoelectroelastic materials [43–46], thus illustrating the capabilities of discontinuous quarter-point elements for SIFs computation. In this paper, the use of such discontinuous quarter-point elements in a dual BEM context is revisited, with the objective of establishing whether they are suitable for T-stress computation as well. To this aim, T-stress will be directly evaluated from the computed nodal displacements at the crack-line nodes and from the stresses evaluated at internal points located in the vicinity of the crack-tip, yielding satisfactory results. The remainder of this paper is organized as follows: the dual BEM formulation employed and the implementation of discontinuous quarter-point elements is summarized in Section 2 to ensure the paper is as self-contained as possible; while Section 3 is devoted to derive the (SIFs and) T-stress computation formulas that are employed in Section 4 to obtain some numerical results that permit to validate our proposal and characterize some key aspects of its practical implementation, like mesh dependence. Finally, Section 5 draws the main conclusions of this study.

2. Dual BEM formulation for crack problems: discontinuous quarter point elements

2.1. Dual BEM approach

Let Ω be homogeneous, linear, elastic and isotropic 2-D cracked domain with external boundary $\Gamma = \Gamma_c \cup \Gamma^+ \cup \Gamma^-$, where Γ_c denotes the non-cracked boundary and $\Gamma^+ \cup \Gamma^-$ stand for the two coincident crack faces, as Fig. 1.b depicts. The dual BEM formulation [42,47–49] applies the classical displacement Boundary Integral Equation (uBIE) on collocation nodes ξ at Γ_c and either one of the crack faces, say $\xi \in \Gamma_+$,

$$c_{ij}(\xi)u_j(\xi) + \int_\Gamma p^*_{ij}(\mathbf{x},\xi)u_j(\mathbf{x})d\Gamma(\mathbf{x}) = \int_\Gamma u^*_{ij}(\mathbf{x},\xi)p_j(\mathbf{x})d\Gamma(\mathbf{x}) \tag{6}$$

whilst the traction Boundary Integral Equation (pBIE) is applied on collocation nodes belonging to the other crack face $\xi \in \Gamma_-$

$$c_{ij}(\xi)p_j(\xi) + N_j(\xi)\int_\Gamma s^*_{ijk}(\mathbf{x},\xi)u_k(\mathbf{x})d\Gamma(\mathbf{x}) = N_j(\xi)\int_\Gamma d^*_{ijk}(\mathbf{x},\xi)p_k(\mathbf{x})d\Gamma(\mathbf{x}) \tag{7}$$

to yield a complete system of equations to determine displacement and tractions on the whole boundary Γ. This dual collocation scheme resolves the ill-conditioning that would result from applying the uBIE on both crack faces, thus providing a single-domain BEM formulation. In Eqs. (6) and (7), absence of body forces is assumed, while all subscripts adopt values $i, j, k = 1, 2$ and the summation rule on repeated indices is implied; u^*_{ij} and p^*_{ij} are the Green's function displacements and boundary tractions, respectively; $N_j(\xi)$ stands for the components of the outward unit normal at the collocation node ξ; and $c_{ij}(\xi)$ is the so-called free term, that takes the values $c_{ij}(\xi) = \delta_{ij}$ when ξ is an internal point and $c_{ij}(\xi) = \frac{1}{2}\delta_{ij}$ for a smooth boundary point, with δ_{ij} standing for Kronecker's delta. The pBIE (7) follows from differentiation of the uBIE (6) with respect to ξ_k and its subsequent substitution into the material constitutive law, so that s^*_{ijk} and d^*_{ijk} are directly obtained by differentiation of p^*_{ij} and u^*_{ij}, respectively.

In this paper, the dual BEM approach as implemented in Sáez et al. [42] will be considered, so that the interested reader is referred to that paper for the expressions of the Green's function and its derivatives together with a thorough discussion on the practical implementation of the approach for fracture problems. In particular, [42] details simple and accurate regularization schemes to deal with the singular and hypersingular integrals arising when evaluating the uBIE and pBIE for boundary collocation nodes. Meshing strategy follows [42] and it is schematized in Fig. 1.b, so that discontinuous quadratic elements are considered to mesh the crack lines in order to guarantee the C^1 continuity of displacements required to compute the pBIE, with the ones at the crack-tip being discontinuous quarter-point elements; standard (continuous) isoparametric quadratic elements are used for the rest of the boundary, except at intersections between a crack-line and any external boundary, where transition semi-discontinuous elements are placed onto the outer boundary.

2.2. Discontinuous quarter-point boundary element

In order to capture the asymptotic $\sqrt{r}$ behavior that the displacement field exhibits near the crack-tip, straight line quarter-point quadratic boundary elements are located at the crack-tip. This elements are simply generated by placing the mid-element node at a distance $L/4$ from the crack-tip, with L being the element length, as Fig. 2.a illustrates.

In this figure, N1 (crack-tip node), N2 and N3 denote the geometrical nodes employed to define the geometry, while NC1, NC2 and NC3 denote the collocation nodes (where the BIEs are applied and the field variables computed) and ζ is the element dimensionless natural coordinate. It is well-known that in the quarter-point element (see for

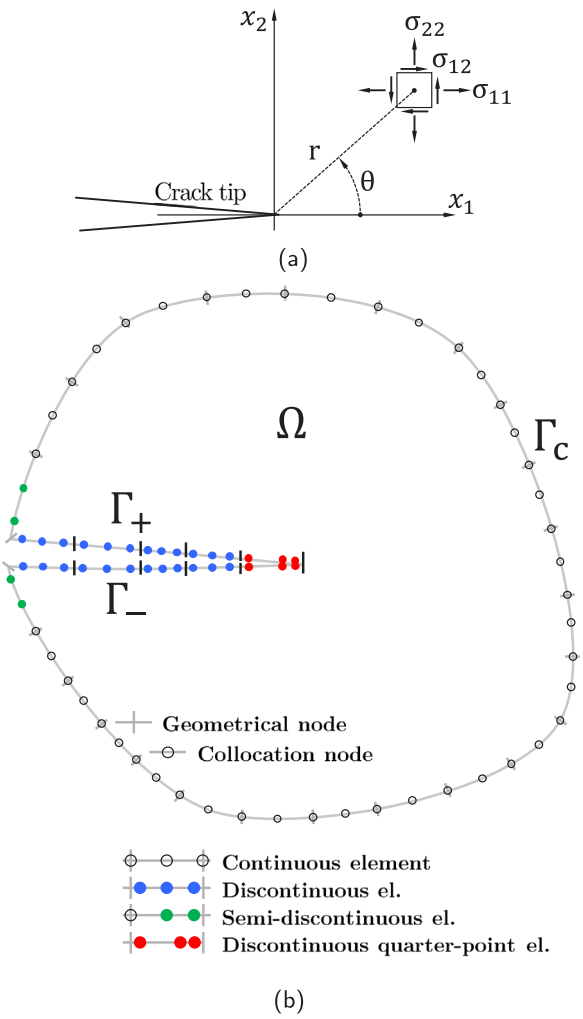

Fig. 1. (a) Local coordinate system at crack tip; (b) Dual BEM discretization of a cracked 2D specimen.

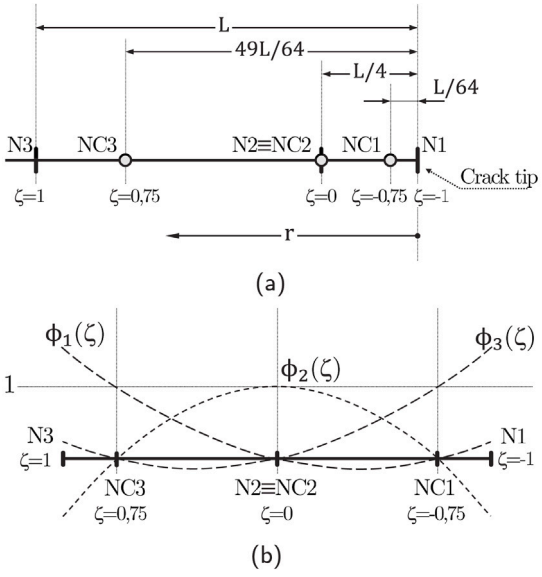

Fig. 2. (a) Quadratic discontinuous quarter-point element; (b) Quadratic interpolation shape functions for the boundary variables at discontinuous elements.

instance [42]) the following relation holds between ζ and the distance r to the crack-tip along the element

$$\zeta = 2\sqrt{\frac{r}{L}} - 1 \tag{8}$$

resulting into the following approximation for the displacement field

$$\begin{aligned} u_k(\zeta) =& u_k^1\phi_1(\zeta) + u_k^2\phi_2(\zeta) + u_k^3\phi_3(\zeta) \\ \Rightarrow u_k =& A + B\sqrt{\frac{r}{L}} + C\frac{r}{L} \end{aligned} \tag{9}$$

where $\phi_i(\zeta)$ are the quadratic element interpolation functions (Fig. 2.b), u_k^i are the values of the displacements at the collocation nodes and, therefore, coefficients A, B and C can be expressed as linear combinations of u_k^i. In particular, for the case in which the collocation nodes are located at $\zeta_1 = -3/4$ ($r_1 = L/64$), $\zeta_2 = 0$ ($r_2 = L/4$) and $\zeta_3 = +3/4$ ($r_3 = L/64$) (with the crack-tip being located at $\zeta = -1$ ($r = 0$), as Fig. 2.a depicts), such coefficients are

$$\begin{aligned} \begin{pmatrix} u_k^1 \\ u_k^2 \\ u_k^3 \end{pmatrix} &= \begin{pmatrix} A & B\sqrt{\frac{r_1}{L}} & C\frac{r_1}{L} \\ A & B\sqrt{\frac{r_2}{L}} & C\frac{r_2}{L} \\ A & B\sqrt{\frac{r_3}{L}} & C\frac{r_3}{L} \end{pmatrix} \\ \Rightarrow \begin{pmatrix} A \\ B \\ C \end{pmatrix} &= \frac{1}{9}\begin{pmatrix} 14 & -7 & 2 \\ -44 & 64 & -20 \\ 32 & -64 & 32 \end{pmatrix}\begin{pmatrix} u_k^1 \\ u_k^2 \\ u_k^3 \end{pmatrix} \end{aligned} \tag{10}$$

It shall be remarked that the generality of the integration scheme proposed in [42] permits to deal with any general straight or curved boundary element with no additional effort involved.

3. T-stress and SIFs computation

Previous studies reveal that extrapolation formulas to directly obtain the SIFs from the Crack Opening Displacements (CODs) at the collocation nodes of discontinuous quarter-point elements are robust and accurate [42,43]. While this technique will be summarized in this section for completeness, new formulas to evaluate T-stress from the computed nodal variables will be presented and its performance and accuracy will be assessed through several numerical examples in the following section.

3.1. SIFs computation

In Ref. [42], the authors present and validate several formulas to evaluate the SIFs directly from the CODs. In particular, one-point formulas that obtain the SIFs from the CODs at the collocation node closest to the crack-tip (NC1) are quite precise and exhibit little mesh dependence. Such formulas follow from particularizing Eqs. (4) and (5) for points along the crack-line ($\theta = \pm\pi$), which for instance for plain strain conditions leads to (neglecting the higher order terms)

$$\begin{pmatrix} \Delta u_1 \\ \Delta u_2 \end{pmatrix} = \begin{pmatrix} u_1^+ - u_1^- \\ u_2^+ - u_2^- \end{pmatrix} = \frac{4(1-\nu)}{\mu}\sqrt{\frac{r}{2\pi}}\begin{pmatrix} K_{II} \\ K_I \end{pmatrix} \tag{11}$$

where superscripts + and − denote the upper and lower crack lines, respectively. Setting $r = L/64$ yields the following one-point formulas to estimate the mode-I and II SIFs

$$\begin{pmatrix} K_I^{NC1} \\ K_{II}^{NC1} \end{pmatrix} = \frac{2\mu}{1-\nu}\sqrt{\frac{2\pi}{L}}\begin{pmatrix} \Delta u_2^{NC1} \\ \Delta u_1^{NC1} \end{pmatrix} \tag{12}$$

from the computed displacements at collocation node NC1. Similar one-point formulas could be obtained for the collocation nodes NC2 or NC3, although SIFs extrapolated from the CODs at the closest collocation node to the crack-tip (NC1), where the $\sqrt{r}$ behavior dominates the asymptotic CODs behavior, yields the best option [42].

Alternative two-point formulas (see [42] for details) or three-point formulas may be derived to evaluate the SIFs by adjusting the variation of the $\sqrt{r}$-term of the displacements along the discontinuous quarter-point crack-tip element, defined by coefficient B in Eqs. (9) and (10), to the corresponding term of the asymptotic displacement expansion given by Eqs. (4) and (5). In this manner, the following three-point formula can be obtained to evaluate the SIFs from the nodal displacements at the three collocation nodes (NC1, NC2, NC3) of the discontinuous quarter-point element

$$\begin{aligned} \begin{pmatrix} K_I^{NC123} \\ K_{II}^{NC123} \end{pmatrix} =& \frac{\mu}{36(1-\nu)}\sqrt{\frac{2\pi}{L}}\times \\ & \begin{pmatrix} -44\Delta u_2^{NC1} + 64\Delta u_2^{NC2} - 20\Delta u_2^{NC3} \\ -44\Delta u_1^{NC1} + 64\Delta u_1^{NC2} - 20\Delta u_1^{NC3} \end{pmatrix} \end{aligned} \tag{13}$$

3.2. T-stress computation

Analogous expressions may be derived to compute the T-stress. For instance, following a similar approach to that of Tan and Wang [33] or Sladek et al. [18], by adjusting the variation of the r-term of the displacements along the discontinuous quarter-point crack-tip element, defined by coefficient C in Eqs. (9) and (10), to the corresponding term of the asymptotic displacement series (4)–(5), the following three-point formula can be derived, for plain strain conditions, in terms of the nodal displacements at the three collocation nodes (NC1, NC2, NC3) of the discontinuous quarter-point element

$$T^{NC123} = \frac{-E}{1-\nu^2}\frac{1}{9L}\left(32u_1^{NC1} - 64u_1^{NC2} + 32u_1^{NC3}\right) \tag{14}$$

Alternatively, extending to BEM the displacement approach suggested in a FEM context by Ayatollahi et al. [10], the T-stress in mixed mode loading may be determined from the nodal displacements at two collocation nodes located along the crack-line on both its upper and lower faces. It follows from Eq. (4) that the sum of the nodal displacements at the upper, $u_1^+ = u_1(r, \theta = +\pi)$, and lower, $u_1^- = u_1(r, \theta = -\pi)$, crack faces in the local x_1-direction (Fig. 1.a) is given as – for the case of plane strain and neglecting the higher order terms –

$$u_1^+ + u_1^- = 2u_{10} - 2\frac{1-\nu^2}{E}Tr \tag{15}$$

so that considering the difference in the values of $u_1^+ + u_1^-$ between two collocation nodes along the crack line, say nodes I and J, located at distances r_I and r_J from the crack-tip, the T-stress can be evaluated from

$$T^{IJ} = \frac{-E}{2(1-\nu^2)}\frac{1}{r_I - r_J}\left[(u_{1I}^+ + u_{1I}^-) - (u_{1J}^+ + u_{1J}^-)\right] \tag{16}$$

In the case of a mode-I crack, the above expression (16) simplifies to

$$T^{IJ} = \frac{-E}{1-\nu^2}\frac{1}{r_I - r_J}\left(u_{1I}^+ - u_{1J}^+\right) \tag{17}$$

T-stress may be as well computed from the stresses evaluated at internal points once the boundary value problem has been solved, following a similar approach to that previously proposed in [10] or [32]. In particular, for internal points located along the crack line, ahead of the crack-tip and quite close to the tip ($\theta = 0$), Eqs. (1) and (2) lead to

$$T^{\sigma} = \left(\sigma_{11} - \sigma_{22}\right)_{\theta=0} \tag{18}$$

Although this last method requires some postprocessing, it implies little computational effort when compared to interaction integral approaches.

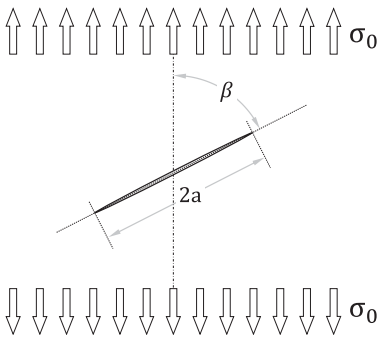

Fig. 3. Inclined crack under tensile loading in an unbounded domain.

4. Numerical results and discussion

This section presents and discuss results obtained for several examples involving both finite and unbounded cracked specimens under pure mode-I and mixed-mode loading conditions. Although emphasis will be placed on T-stress evaluation, data illustrating SIFs computation will be as well included, so that the reader may get a clear picture of the potential, accuracy and robustness of the proposed methods to compute both fracture parameters. The material considered in all the examples corresponds to a 0.50 wt% Multi Walled Carbon NanoTube (MWCNT)/epoxy composite, whose elastic moduli are computed by a core–shell micromechanics approach (see García-Macías et al. for details [50]). This interphase model assumes that interfacial properties can be idealized as finite elastic coatings with constant thickness t surrounding the fillers and computes the homogenized properties at a Representative Volume Element (RVE) adopting invariant geometrical dimensions of the MWCNTs throughout the RVE, resulting into a homogeneous and isotropic material description with effective properties: $E = 2.86$ GPa and $\nu = 0.28$. At any event, any arbitrary values could be adopted for this validation examples, provided that the values of the coefficients of the Williams expansion are independent of the material constants for homogeneous materials [17,20].

4.1. Inclined crack in an unbounded domain

The first example corresponds to an inclined crack of length $2a$ immersed in an unbounded domain and subjected to a uniaxial far-field stress σ_0, as Fig. 3 illustrates. For this configuration, the analytical solution is given by (see for instance [5])

$$\begin{aligned} K_I &= \sigma_0\sqrt{\pi a}\sin^2\beta \\ K_{II} &= \sigma_0\sqrt{\pi a}\sin\beta\cos\beta \\ T &= \sigma_0\cos 2\beta \end{aligned} \tag{19}$$

For a mixed-mode crack with inclination $\beta = 60°$, Fig. 4 depicts the computed values of the T-stress and the SIFs for different boundary element meshes, ranging from 5 to 80 uniform (same size) quadratic elements on the crack line. T-stress is evaluated from the obtained nodal displacements at the 3 collocation nodes of the discontinuous quarter-point element (T^{NC123}) using Eq. (14), whilst K_I and K_{II} are determined employing both: (i) the one-point formula based on the computed nodal crack opening displacements (CODs) at the collocation node closest to the crack-tip ($NC1$: K^{NC1}), as derived in Eq. (12); and (ii) the three-point formula given by Eq. (13), based on the CODs at the three nodes of the discontinuous quarter-point element (K^{NC123}). All the values are normalized against their analytical counterparts (Eq. (19)). As previous studies already revealed [42,43], the SIFs obtained using the one-point formula are quite stable and converge for rather coarse meshes, leading to good results even for a 5 element mesh. However, the SIFS obtained using the three point formula exhibit

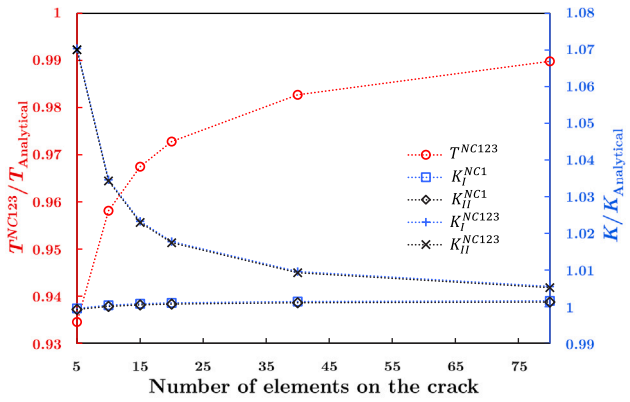

Fig. 4. Normalized T-stress (T^{NC123}) and SIFs versus number of elements to mesh the crack (uniform meshes). Inclined crack in infinite domain ($\beta = 60°$).

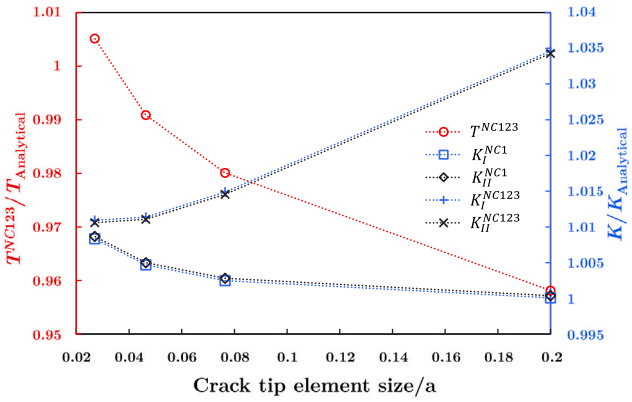

Fig. 5. Normalized T-stress (T^{NC123}) and SIFs versus crack-tip element size for 10 (non-uniform) element mesh. Inclined crack in infinite domain ($\beta = 60°$).

a greater mesh dependence and converge to the expected analytical values only for finer meshes: above 40 elements the discrepancy with the reference solution is below 1%. T^{NC123} exhibits a similar behavior to K^{NC123}: convergence is attained only for fine meshes so that, at least, proper computation of the T-stress requires a mesh that guarantees that the value of K^{NC123} is close to the more stable K^{NC1} value, thus providing a rule of thumb for those cases where analytical solutions are not available.

Fig. 5 illustrates the behavior of these same fracture parameters (T^{NC123}, K^{NC123}, K^{NC1}) for a mesh of 10 elements with varying crack-tip element size (L), so that $L/a = 0.2$ corresponds to the uniform mesh case. It can be observed that good results are obtained for the T-stress provided that L/a is between 0.025 and 0.05, which – as in Fig. 4 – coincides with the range where the three-point formula for the SIFs (K^{NC123}) approaches the results provided by the one-point formula (K^{NC1}).

Regarding the crack mesh, for instance results shown for $L/a = 0.05$ in Fig. 5 correspond to a 10-element mesh with non uniform element sizes, so that the ratio between the sizes of the elements at the center of the crack and at the crack-tip is 10. This figure reveals that the crack-tip element size is the key parameter to ensure the accuracy of the T-stress values directly extrapolated from the computed nodal displacements, when using the three-point formula derived in Eq. (14).

Next, performance of the two-point displacement formula proposed in Eq. (16) is analyzed (T^{IJ}). To this end, collocation node I will be selected always as the closest to the crack tip, NC1 ($I = NC1$), whilst results for collocation nodes J along the crack-line are displayed in Fig. 6 in terms of their distance r_J to the crack-tip, so that for

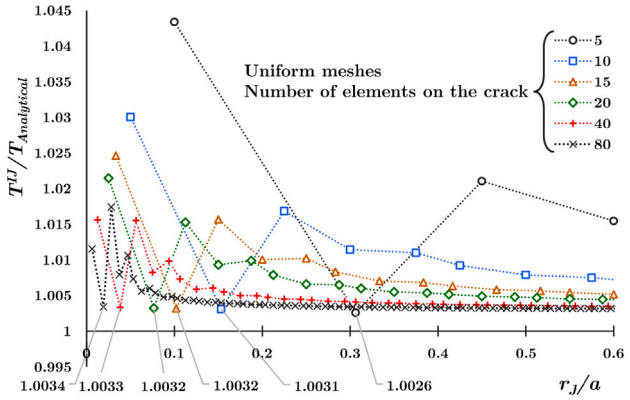

Fig. 6. Normalized T-stress, T^{IJ}, versus distance r_J of collocation node J to the crack-tip (uniform meshes; node $I = NC1$). Inclined crack in infinite domain ($\beta = 60°$).

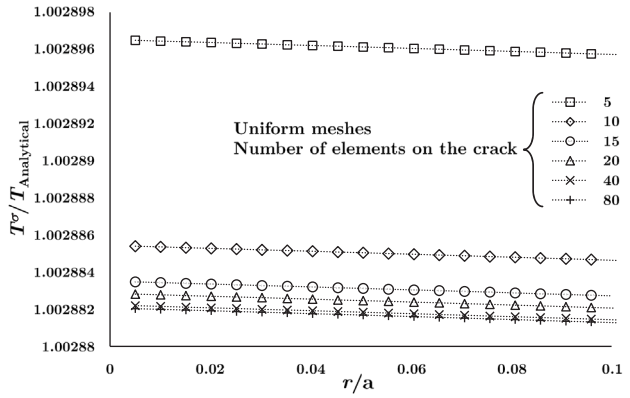

Fig. 7. Normalized T-stress evaluated from stresses at internal points ahead of the crack-tip, T^{σ}, versus distance r of the internal point to the crack-tip (uniform meshes). Inclined crack in infinite domain ($\beta = 60°$).

instance, the first point (lowest r_J) shown in the figure for each mesh corresponds to $J = NC2$, the second point corresponds to $J = NC3$ (NC2 and NC3 being the central and extreme collocation nodes on the quarter-point discontinuous element, as denoted in Fig. 2), the third point corresponds to J coinciding with the first node of the element connected to the quarter-point discontinuous element (denoted here as NC4) and so on. T-stress in Fig. 6 is normalized with respect to its analytical value and the distance to the crack-tip r_J is normalized with respect to the crack half-length a. Results for uniform meshes ranging from 5 to 80 equal-length elements are presented. Fig. 6 reveals that T-stress obtained adopting $I = NC1$ and $J = NC3$ are not only accurate but exhibit little mesh dependence. Results of T^{IJ} obtained for $I = NC1$ and $J = NC4$ or $J = NC2$ should not be considered, as they lead to the less accurate results. T^{IJ} values obtained for collocation nodes J outside the quarter-point element (and different from NC4), although mesh-dependent, provide also a good approximation to the actual T-tress for fine meshes.

Observation of Figs. 5 and 6 concludes that the derived extrapolation formulas for T^{IJ} (with $I = NC1$ and $J = NC3$) clearly outperforms T^{NC123} in terms of both accuracy and mesh dependency.

Normalized T-stress obtained from the computed stresses at internal points located ahead of the crack-tip are depicted in Fig. 7 for several uniform meshes and an inclination angle $\beta = 60°$. Obtained values of T^{σ} (Eq. (18)) are quite stable and exhibit little mesh dependence, with discrepancies with respect to the analytical solution below 0.3% even for a coarse 5 element mesh.

Finally, Tables 1 and 2 summarize the obtained T-stress and SIFs results, respectively, for crack angles ranging from $\beta = 0°$ to $\beta = 90°$,

Table 1
T-stress computed by the proposed formulations for inclined crack in infinite domain under tensile load. Analytical solution adopted for Ref. (Eq. (19)).

Crack angle [°]	T^{σ}/σ_0	T^{IJ}/σ_0	T^{NC123}/σ_0
0	1.0000	1.0000	1.0000
7.5	0.9659	0.9659	0.9660
15	0.8659	0.8659	0.8665
22.5	0.7069	0.7067	0.7081
30	0.4996	0.4994	0.5016
37.5	0.2582	0.2578	0.2612
45	−0.0009	−0.0014	−0.0031
52.5	−0.2600	−0.2606	−0.2549
60	−0.5015	−0.5022	−0.4954
67.5	−0.7088	−0.7097	−0.7020
75	−0.8679	−0.8689	−0.8605
82.5	−0.9680	−0.9690	−0.9601
90	−1.0021	−1.0031	−0.9941
Crack angle [°]	T^{σ}/Ref.	T^{IJ}/Ref.	T^{NC123}/Ref.
0	1.0000	1.0000	1.0000
7.5	1.0000	1.0000	1.0001
15	0.9999	0.9998	1.0005
22.5	0.9997	0.9995	1.0014
30	0.9992	0.9987	1.0032
37.5	0.9976	0.9962	1.0091
45	–	–	–
52.5	1.0045	1.0069	0.9850
60	1.0029	1.0044	0.9909
67.5	1.0024	1.0036	0.9927
75	1.0022	1.0033	0.9936
82.5	1.0021	1.0031	0.9940
90	1.0021	1.0031	0.9941

adopting the analytical solution in Eq. (19) as reference. Results for T^{σ} are computed at an internal point located at a distance $r = 2a/500$ ahead of the crack-tip, while T^{IJ} are computed adopting $I = NC1$ and $J = NC3$. A 10-elements non-uniform mesh with the crack-tip element size being $L/a = 0.025$ has been considered for all the cases. Excellent agreement with the analytical solution, for both T-stress and SIFs, is observed for all the inclination angles β.

4.2. Inclined edge crack in a rectangular plate

The following example considers a finite rectangular plate with an inclined edge crack, as Fig. 8 illustrates. The geometry of the problem is defined by $h = w$, $a = 0.6$ w and $\beta = 60°$. The plate is subjected to a uniform tensile stress of magnitude σ_0 applied onto its upper and lower edges. The quadratic boundary element mesh consists of 60 equally sized elements on the non-cracked boundary plus 10 elements on the crack, with the element at the crack-tip being discontinuous quarter-point. This problem has been previously solved by other authors using different numerical techniques, as Table 3 summarizes. In particular, the results obtained by Hou et al. [20] using the finite element package ABAQUS will be adopted as the reference solution in our study.

Fig. 9 depicts the values of T-stress and SIFs obtained using a 10-element mesh on the crack with varying crack-tip element size (L): $L/a = 0.1$ corresponds to the uniform mesh case while, for instance, $L/a = 0.015$ corresponds to a non-uniform mesh with a ratio between the sizes of the elements at the edge of the plate and at the crack-tip of 20. Results for T^{IJ} are obtained adopting collocation node NC1 as node I and collocation node NC3 of the quarter-point element as node J, whilst T^{σ} is computed from the stresses at an internal point located at a distance $r = a/500$ ahead of the crack tip, following the conclusions drawn from the previous example. Once again, the one-point formula for the SIFs (K^{NC1}), Eq. (12), exhibits good accuracy and stability for all the considered meshes, while the three-point formula for the SIFs (K^{NC123}), Eq. (13), does only lead to values within 1% of the reference solution for small crack-tip element sizes, say $L/a \leq 0.025$. Regarding the T-stress values, similar conclusions to those obtained in the previous example may be extracted: (i) T^{σ} provides accurate and stable results

Table 2
Normalized SIFs ($K_*/\sigma_0\sqrt{\pi a}$) computed by one and three point CODs formulas for inclined crack in infinite domain under tensile load. Analytical solution adopted for Ref. (Eq. (19)).

Crack angle [°]	K_I^{NC1}	K_{II}^{NC1}	K_I^{NC123}	K_{II}^{NC123}
0	0.0000	0.0000	0.0000	0.0000
7.5	0.0171	0.1300	0.0172	0.1308
15	0.0673	0.2511	0.0677	0.2527
22.5	0.1471	0.3551	0.1481	0.3574
30	0.2512	0.4350	0.2528	0.4377
37.5	0.3724	0.4852	0.3748	0.4882
45	0.5025	0.5023	0.5056	0.5055
52.5	0.6325	0.4852	0.6365	0.4883
60	0.7538	0.4350	0.7585	0.4378
67.5	0.8579	0.3552	0.8633	0.3575
75	0.9377	0.2512	0.9437	0.2528
82.5	0.9880	0.1300	0.9942	0.1309
90	1.0051	0.0000	1.0115	0.0000
Crack angle [°]	$\frac{K_I^{NC1}}{\text{Ref.}}$	$\frac{K_{II}^{NC1}}{\text{Ref.}}$	$\frac{K_I^{NC123}}{\text{Ref.}}$	$\frac{K_{II}^{NC123}}{\text{Ref.}}$
0	–	–	–	–
7.5	1.0047	1.0044	1.0111	1.0108
15	1.0047	1.0044	1.0111	1.0108
22.5	1.0048	1.0045	1.0112	1.0108
30	1.0048	1.0045	1.0112	1.0109
37.5	1.0049	1.0045	1.0112	1.0109
45	1.0049	1.0046	1.0113	1.0110
52.5	1.0050	1.0046	1.0113	1.0110
60	1.0050	1.0047	1.0114	1.0111
67.5	1.0050	1.0047	1.0114	1.0111
75	1.0051	1.0048	1.0114	1.0111
82.5	1.0051	1.0048	1.0115	1.0111
90	1.0051	–	1.0115	–

Table 3
T-stress and SIFs for rectangular plate with an inclined edge crack, obtained by different numerical techniques.

Reference	T/σ_0	K_I	K_{II}
Hou et al. [20] ODM	0.6078	11.02111	2.9937
Hou et al. [20] ABAQUS	0.6019	11.03	2.998
Karihaloo et al. [51] HCE	0.5852	10.4278	2.829
Karihaloo et al. [51] BCM	0.594	10.4662	2.8403

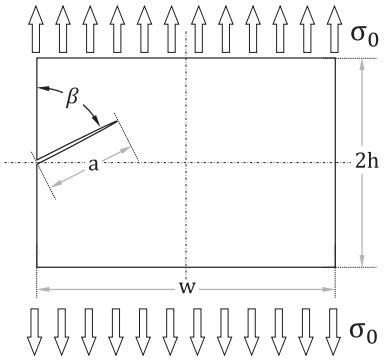

Fig. 8. Inclined edge crack in a rectangular plate.

with negligible mesh dependence; (ii) small crack-tip element sizes are required in order to capture T-stress using the displacement formulas for T^{NC123}, Eq. (14), and T^{IJ}, Eq. (16) and, furthermore, T^{NC123} exhibits a greater mesh dependence and does only converge to the reference T-stress value when the SIFs values obtained using K^{NC123} converge to those evaluated using K^{NC1}, while T^{IJ} produces more stable results for all the considered crack-tip sizes and leads to quite accurate results for $L/a \leq 0.01$, so that finer meshes are required to compute the T-stress than those necessary to evaluate the SIFs. Once again, T^{IJ} outperforms T^{NC123} and provides good approximation to the T-stress from direct extrapolation of the computed nodal displacements.

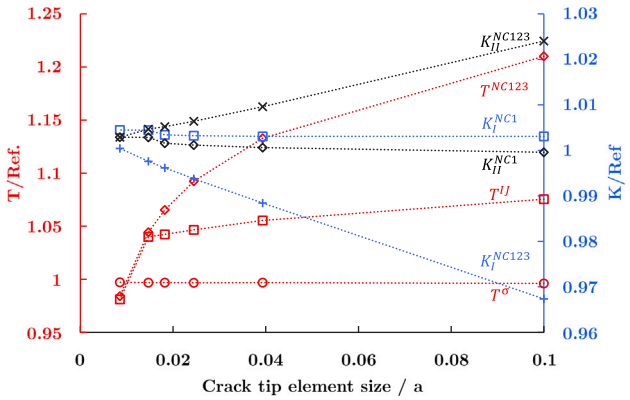

Fig. 9. Normalized T-stress and SIFs versus crack-tip element size. Rectangular plate with inclined edge crack.

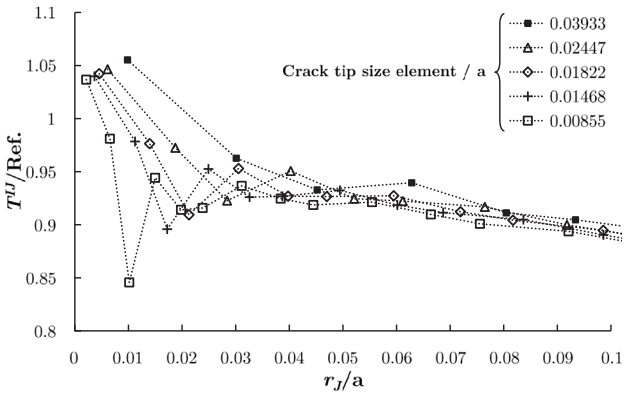

Fig. 10. Normalized T-stress, T^{IJ}, versus distance r_J from collocation node J to the crack-tip (node I is NC1). Results for 10-element mesh on the crack and varying crack-tip element size. ABAQUS results in Table 3 adopted as Ref. solution. Rectangular plate with an inclined edge crack.

Tables 4 and 5 present the same results in tabular format for the T-stress and SIFs, respectively.

Fig. 10 illustrates the behavior of the T^{IJ} formula to compute the T-stress for different non-uniform meshes of 10 elements along the crack, adopting NC1 (closest node to the crack-tip) as the collocation node I and varying the collocation node J along the crack line (identified by their dimensionless distance to the crack-tip r_J/a) so that, for instance, the first point (lowest r_J/a) in Fig. 10 – for each mesh – corresponds to $J = NC2$, the second point corresponds to $J = NC3$ (see Fig. 2) and so on. Similar conclusions as those obtained in the previous example may be drawn: results obtained adopting $I = NC1$ and $J = NC3$ are the most accurate and exhibit little mesh dependence.

4.3. Mode-I single edge notched (SEN) specimen

A horizontal edge crack in a rectangular plate is next considered. The geometry is illustrated in Fig. 8, with $h = \text{w}$ and $\beta = 90°$, so that only mode-I crack behavior is excited by the uniaxial stress loading σ_0. In this case, crack lengths ranging from $a/\text{w} = 0.1$ to 0.5 are considered and the solution obtained by Leonetti and Vantadori [52] using weight functions is adopted as reference (Table 6 summarizes the normalized T-stress (T/σ_0) and SIFs ($K_I/\sigma_0\sqrt{\pi a}$) for all the considered a/w ratios). The mesh coincides with the one described in the previous example, with 10 non-uniform elements employed to mesh the crack, with a crack-tip element size $L/a = 0.0085$, as sketched in Fig. 11.

Results for the T-stress and mode-I SIF are favorably compared with the reference solution in Tables 7 and 8, respectively. As in previous

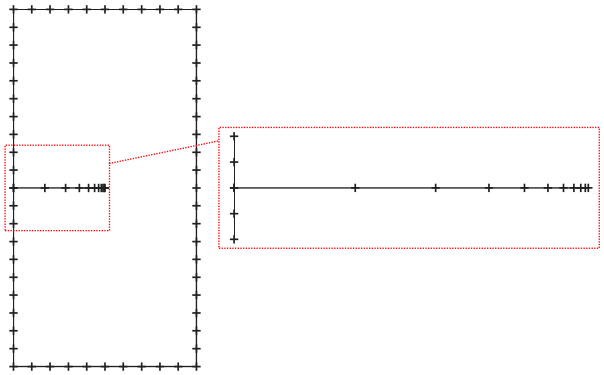

Fig. 11. Boundary element mesh for SEN specimen.

Table 4
T-stress evaluated using the proposed formulation and a 10-element mesh for the crack, with varying crack-tip element size (L). ABAQUS results in Table 3 adopted as Ref. solution. Rectangular plate with an inclined edge crack.

L/a	T^{σ}/σ_0	T^{IJ}/σ_0	T^{NC123}/σ_0
0.1000	0.5996	0.5542	0.7284
0.0393	0.6000	0.5794	0.6819
0.0245	0.6000	0.5854	0.6574
0.0182	0.6000	0.5877	0.6413
0.0147	0.6000	0.5889	0.6286
0.0085	0.6002	0.5905	0.5923
L/a	T^{σ}/Ref.	T^{IJ}/Ref.	T^{NC123}/Ref.
0.1000	0.9961	0.9207	1.2102
0.0393	0.9968	0.9627	1.1329
0.0245	0.9968	0.9726	1.0923
0.0182	0.9968	0.9764	1.0654
0.0147	0.9968	0.9785	1.0444
0.0085	0.9971	0.9811	0.9841

Table 5
SIFs evaluated using the proposed formulation and a 10-element mesh for the crack, with varying crack-tip element size (L). ABAQUS results in Table 3 adopted as Ref. solution. Rectangular plate with an inclined edge crack.

L/a	K_I^{NC1}	K_I^{NC123}	K_{II}^{NC1}	K_{II}^{NC123}
0.1000	11.0643	10.6701	2.9968	3.0701
0.0393	11.0641	10.9022	2.9998	3.0268
0.0245	11.0656	10.9613	3.0015	3.0173
0.0182	11.0679	10.9875	3.0027	3.0137
0.0147	11.0792	11.0034	3.0066	3.0120
0.0085	11.0793	11.0349	3.0068	3.0101
L/a	$\frac{K_I^{NC1}}{\text{Ref.}}$	$\frac{K_I^{NC123}}{\text{Ref.}}$	$\frac{K_{II}^{NC1}}{\text{Ref.}}$	$\frac{K_{II}^{NC123}}{\text{Ref.}}$
0.1000	1.0031	0.9674	0.9996	0.9996
0.0393	1.0031	0.9884	1.0006	1.0006
0.0245	1.0032	0.9938	1.0012	1.0012
0.0182	1.0034	0.9962	1.0016	1.0016
0.0147	1.0045	0.9976	1.0029	1.0029
0.0085	1.0045	1.0004	1.0029	1.0029

examples, T^{σ} is computed from the stresses at an internal point located at a distance $r = a/500$ ahead of the crack-tip. T^{IJ} is computed adopting $I = NC1$ and $J = NC3$ (extreme nodes on the discontinuous quarter-point element, Fig. 2). Agreement for the mode-I SIF is excellent in all the cases. Regarding T-stress, both T^{σ} and T^{IJ} provide excellent results, while T^{NC123} exhibits larger discrepancies for $a/\text{w} = 0.4, 0.5$. These discrepancies reduce to acceptable limits in case of employing finer meshes. At any event, T^{IJ} outperforms T^{NC123} and provides a valid extrapolation formula for all the considered examples.

Table 6
Normalized T-stress and mode-I SIF for SEN specimen. Weight functions solution adopted as Ref. [52].

a/w	T/σ_0	$K_I/\sigma_0\sqrt{\pi a}$
0.1	−0.5500	1.1899
0.2	−0.5890	1.3682
0.3	−0.6080	1.6610
0.4	−0.5710	2.1123
0.5	−0.4100	2.8249

Table 7
Normalized T-stress using the proposed formulation and a 10-element non-uniform mesh on the crack. SEN specimen (see Table 6 for Ref. results).

a/w	$\frac{T^{\sigma}}{\sigma_0}$	$\frac{T^{IJ}}{\sigma_0}$	$\frac{T^{NC123}}{\sigma_0}$	$\frac{T^{\sigma}}{\text{Ref.}}$	$\frac{T^{IJ}}{\text{Ref.}}$	$\frac{T^{NC123}}{\text{Ref.}}$
0.1	−0.5494	−0.5490	−0.5524	0.9990	0.9982	1.0044
0.2	−0.5893	−0.5890	−0.5942	1.0004	1.0001	1.0089
0.3	−0.6081	−0.6085	−0.6182	1.0001	1.0009	1.0167
0.4	−0.5711	−0.5730	−0.5925	1.0001	1.0036	1.0376
0.5	−0.4091	−0.4146	−0.4559	0.9979	1.0113	1.1120

Table 8
Normalized mode-I SIF ($K_I/\sigma_0\sqrt{\pi a}$) using one and three-point formulas, for different crack sizes. SEN specimen (see Table 6 for Ref. results).

a/w	K_I^{NC1}	K_I^{NC123}	$\frac{K_I^{NC1}}{\text{Ref.}}$	$\frac{K_I^{NC123}}{\text{Ref.}}$
0.1	1.1947	1.1946	1.0040	1.0039
0.2	1.3720	1.3716	1.0028	1.0025
0.3	1.6661	1.6649	1.0031	1.0024
0.4	2.1196	2.1166	1.0034	1.0020
0.5	2.8352	2.8280	1.0037	1.0011

4.4. Circular arched crack in an unbounded domain

The last example corresponds to a circular arched crack, of radius R and semi-angle α, immersed in an infinite plate and subjected to a bidirectional tensile far field stress of magnitude σ_0, as Fig. 12 depicts.

This example aims at illustrating the performance of the proposed approach when dealing with curved crack geometries. Cracks with semi-angles ranging from $\alpha = 30°$ to $\alpha = 90°$ will be next considered. Boundary element meshes consisting of 20 discontinuous quadratic elements are used for all the cases: 18 curved quadratic elements plus 2 quite small quarter-point straight elements at the tips (i.e., so that $L/a \leq 0.01$, with L being the size of the element at the crack-tip and a being the crack length). Numerical results obtained for both SIFs and T-stress are favorably compared with Cotterell and Rice's [53] and Chen's [54] analytical solutions, respectively, in Fig. 13. Only results evaluated by direct extrapolation from the computed nodal displacements are presented in Fig. 13. T^{NC123} and T^{IJ} are computed, respectively, according to Eqs. (14) and (16) whilst K^{NC1} and K^{NC123} are evaluated using Eqs. (12) and (13), respectively. As in previous examples, for T^{IJ} computations, collocation node I is selected as NC1, whilst node J is adopted as NC3 in the quarter-point element (see Fig. 2). The conclusions drawn for this case are identical to those of the previous cases.

5. Conclusions

This paper extends the formulation of the dual BEM in conjunction with the use of discontinuous quarter-point elements to obtain T-stress in fracture mechanics applications. To this end, new extrapolation formulas are derived to directly evaluate the T-stress from the computed nodal displacements at the collocation nodes of the discontinuous quarter-point element. T-stress is also evaluated from the computed stresses at internal points. The use of quarter-point discontinuous quadratic boundary elements had proven quite effective, in previous works by the authors [42–45], to evaluate SIFs and, herein, its

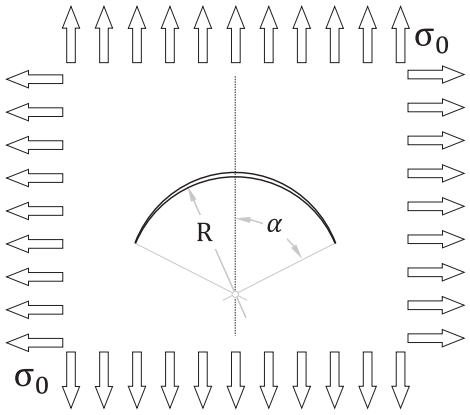

Fig. 12. Arc-shaped crack under bidirectional tensile loading in an unbounded domain.

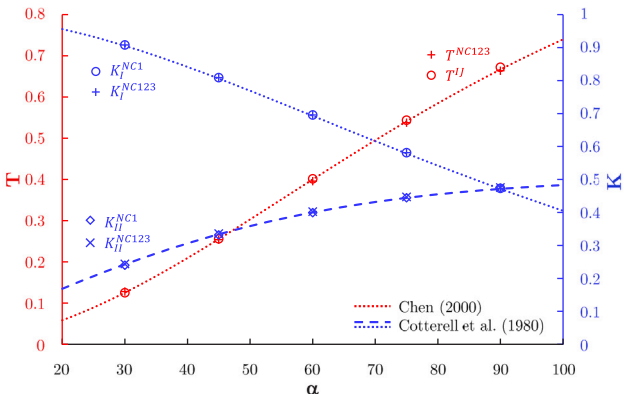

Fig. 13. T-stress and SIF's vs. crack semi-angle α. Circular arched crack in infinite domain.

adequacy to further compute T-stress has been addressed and validated via several numerical examples involving both mode-I and mixed mode crack configurations. Although the main objective of the paper focuses on the calculation of T-stress in planar isotropic media, results for the SIFs have also been included for the sake of completeness. The main conclusions of this study are:

- The use of discontinuous quarter-point boundary elements in a dual BEM context permits an effective and accurate evaluation of both SIFs and T-stress by direct extrapolation from the computed nodal displacements.
- To evaluate the SIFs, the one-point formula derived in Eq. (12) leads to a quite precise procedure to compute the SIFs in terms of the COD at the collocation node of the quarter-point element that is located next to the crack-tip (NC1 in Fig. 2): K^{NC1}. This procedure produces accurate results even for rather coarse meshes. The alternative three-point formula derived in Eq. (13) to extrapolate the SIFs in terms of the CODs at the three collocation nodes of the quarter-point discontinuous element (NC1, NC2 and NC3 in Fig. 2) leads to SIFs values (K^{NC123}) that only converge for finer meshes and exhibit a strong mesh dependence. Therefore, K^{NC1} is the recommended procedure to evaluate the SIFs.
- Three procedures have been proposed and analyzed for T-stress computation:
  - T^{NC123}: The three-point formula derived in Eq. (14) allows to extrapolate the T-stress from the nodal displacements at the three collocation nodes of the quarter-point element. This procedure requires finer meshes than those needed for SIFs computation and exhibits a strong mesh dependence. Accurate results can only be obtained for meshes that ensure that, at least, the SIFs computed using K^{NC123} converge to the values obtained using K^{NC1}.
  - T^{IJ}: The two-point formula derived in Eq. (16) permits to extrapolate the T-stress from the nodal displacements of any two collocation nodes I and J along the crack faces. When node I is selected as NC1 and node J as NC3 in the quarter-point element (see Fig. 2), optimal results with limited mesh dependence are obtained. T^{IJ} outperforms T^{NC123} in all the numerical examples analyzed. Accurate results are obtained even for rather coarse meshes (10 elements on the crack), provided that the ratio of the size of the element at the crack-tip (L) to the crack length (a) is $L/a \leq 0.01$, thus leading to a non-uniform mesh.
  - T^{σ}: The formula derived in Eq. (18) evaluates the T-stress from the computed stresses at any internal point located along the crack line and ahead of the crack-tip. Stable and accurate results are obtained for even rather coarse meshes. In this work, we evaluate T^{σ} at a point located at a distance $r = a/500$ from the crack-tip. Although this procedure requires some additional postprocessing when compared to the extrapolation procedures (T^{IJ}, T^{NC123}), it still implies little computational effort in comparison with the interaction integral approaches.

In conclusion, both T^{IJ} and T^{σ} are efficient and accurate procedures to determine the T-stress that can be implemented quite straightforwardly in a dual BEM context using discontinuous quarter-point quadratic boundary elements.

CRediT authorship contribution statement

C. Baena: Software, Formal analysis, Investigation, Writing – original draft. **F. García-Sánchez:** Software, Formal analysis, Investigation, Funding acquisition, Editing. **A. Sáez:** Conceptualization, Methodology, Investigation, Funding acquisition, Writing – original draft & review.

Declaration of competing interest

The authors declare the following financial interests/personal relationships which may be considered as potential competing interests: Felipe Garcia-Sanchez reports financial support was provided by Ministerio de Ciencia, Innovación y Universidades of Spain and European Regional Development Fund (RTI2018-094945-B-C21). Andres Saez reports financial support was provided by Consejería de Economía y Conocimiento of Andalucía (Spain) and European Regional Development Fund (P18-RT-3128). Andres Saez reports financial support was provided by Ministerio de Ciencia, Innovación y Universidades of Spain and European Regional Development Fund (RTI2018-094945-B-C21).

Data availability

No data was used for the research described in the article.

Acknowledgments

This work was supported by the Ministerio de Ciencia, Innovación *y* Universidades of Spain, the European Regional Development Fund and the Consejería de Economía *y* Conocimiento of Andalucía (Spain) under projects RTI2018-094945-B-C21 and P18-RT-3128. Partial funding for open access charge: Universidad de Málaga / CBUA. The financial support is gratefully acknowledged.

References

[1] M. Williams, On the stress distribution at the base of a stationary crack, J. Appl. Mech. 24 (1) (1957) 109–114.

[2] B. Karihaloo, Q. Xiao, Accurate determination of the coefficients of elastic crack tip asymptotic field by a hybrid crack element with p-adaptivity, Eng. Fract. Mech. 68 (15) (2001) 1609–1630, http://dx.doi.org/10.1016/S0013-7944(01)00063-7.

[3] S. Larsson, A. Carlsson, Influence of non-singular stress terms and specimen geometry on small-scale yielding at crack tips in elastic-plastic materials, J. Mech. Phys. Solids 21 (4) (1973) 263–277, http://dx.doi.org/10.1016/0022-5096(73)90024-0.

[4] C. Betegón, J. Hancock, Two-parameter characterization of elastic-plastic crack-tip fields, J. Appl. Mech. Trans. ASME 58 (1) (1991) 104–110, http://dx.doi.org/10.1115/1.2897135.

[5] D. Smith, M. Ayatollahi, M. Pavier, The role of T-stress in brittle fracture for linear elastic materials under mixed-mode loading, Fatigue Fract. Eng. Mater. Struct. 24 (2) (2001) 137–150, http://dx.doi.org/10.1046/j.1460-2695.2001.00377.x.

[6] D. Smith, M. Ayatollahi, M. Pavier, On the consequences of T-stress in elastic brittle fracture, Proc. R. Soc. Lond. Ser. A Math. Phys. Eng. Sci. 462 (2072) (2006) 2415–2437, http://dx.doi.org/10.1098/rspa.2005.1639.

[7] M. Ayatollahi, M. Rashidi Moghaddam, F. Berto, A generalized strain energy density criterion for mixed mode fracture analysis in brittle and quasi-brittle materials, Theor. Appl. Fract. Mech. 79 (2015) 70–76, http://dx.doi.org/10.1016/j.tafmec.2015.09.004.

[8] M. Gupta, R. Alderliesten, R. Benedictus, A review of T-stress and its effects in fracture mechanics, Eng. Fract. Mech. 134 (2015) 218–241, http://dx.doi.org/10.1016/j.engfracmech.2014.10.013.

[9] A. Kfouri, Some evaluations of the elastic T-term using Eshelby's method, Int. J. Fract. 30 (4) (1986) 301–315, http://dx.doi.org/10.1007/BF00019710.

[10] M. Ayatollahi, M. Pavier, D. Smith, Determination of T -stress from finite element analysis for mode I and mixed mode I/II loading, Int. J. Fract. 91 (3) (1998) 283–298, http://dx.doi.org/10.1023/A:1007581125618.

[11] M. Acanfora, P. Gallo, S. Razavi, M. Ayatollahi, F. Berto, Numerical evaluation of T-stress under mixed mode loading through the use of coarse meshes, Phys. Mesomech. 21 (2) (2018) 124–134, http://dx.doi.org/10.1134/S1029959918020054.

[12] C.-S. Chen, R. Krause, R. Pettit, L. Banks-Sills, A. Ingraffea, Numerical assessment of T-stress computation using a p-version finite element method, Int. J. Fract. 107 (2) (2001) 177–199, http://dx.doi.org/10.1023/A:1007689311129.

[13] Q. Xiao, B. Karihaloo, X. Liu, Direct determination of SIF and higher order terms of mixed mode cracks by a hybrid crack element, Int. J. Fract. 125 (3–4) (2004) 207–225, http://dx.doi.org/10.1023/b:frac.0000022229.54422.13.

[14] Q. Xiao, B. Karihaloo, Implementation of hybrid crack element on a general finite element mesh and in combination with XFEM, Comput. Methods Appl. Mech. Engrg. 196 (13–16) (2007) 1864–1873, http://dx.doi.org/10.1016/j.cma.2006.09.022.

[15] R. Su, W. Feng, Accurate determination of mode I and II leading coefficients of the williams expansion by finite element analysis, Finite Elem. Anal. Des. 41 (11–12) (2005) 1175–1186, http://dx.doi.org/10.1016/j.finel.2004.11.006.

[16] R. Su, S. Fok, Determination of coefficients of the crack tip asymptotic field by fractal hybrid finite elements, Eng. Fract. Mech. 74 (10) (2007) 1649–1664, http://dx.doi.org/10.1016/j.engfracmech.2006.09.009.

[17] M. Ayatollahi, M. Nejati, An over-deterministic method for calculation of coefficients of crack tip asymptotic field from finite element analysis, Fatigue Fract. Eng. Mater. Struct. 34 (3) (2011) 159–176, http://dx.doi.org/10.1111/j.1460-2695.2010.01504.x.

[18] J. Sladek, V. Sladek, M. Repka, C. Tan, Evaluation of the T-stress for cracks in functionally graded materials by the FEM, Theor. Appl. Fract. Mech. 86 (2016) 332–341, http://dx.doi.org/10.1016/j.tafmec.2016.09.004.

[19] C. Hou, Z. Wang, W. Liang, H. Yu, Z. Wang, Investigation of the effects of confining pressure on SIFs and T-stress for CCBD specimens using the XFEM and the interaction integral method, Eng. Fract. Mech. 178 (2017) 279–300, http://dx.doi.org/10.1016/j.engfracmech.2017.03.049.

[20] C. Hou, Z. Wang, X. Jin, X. Ji, X. Fan, Determination of SIFs and T-stress using an over-deterministic method based on stress fields: Static and dynamic, Eng. Fract. Mech. 242 (2021) http://dx.doi.org/10.1016/j.engfracmech.2020.107455.

[21] Y. Li, K. Zheng, Crack tip asymptotic field coefficients analyses based on extended finite element method using over-deterministic displacement field fitting method, Theor. Appl. Fract. Mech. 113 (2021) http://dx.doi.org/10.1016/j.tafmec.2021.102971.

[22] C. Song, Evaluation of power-logarithmic singularities, T-stresses and higher order terms of in-plane singular stress fields at cracks and multi-material corners, Eng. Fract. Mech. 72 (10) (2005) 1498–1530, http://dx.doi.org/10.1016/j.engfracmech.2004.11.002.

[23] S. Chidgzey, A. Deeks, Determination of coefficients of crack tip asymptotic fields using the scaled boundary finite element method, Eng. Fract. Mech. 72 (13) (2005) 2019–2036, http://dx.doi.org/10.1016/j.engfracmech.2004.07.010.

[24] C. Song, Z. Vrcelj, Evaluation of dynamic stress intensity factors and T-stress using the scaled boundary finite-element method, Eng. Fract. Mech. 75 (8) (2008) 1960–1980, http://dx.doi.org/10.1016/j.engfracmech.2007.11.009.

[25] C. Song, E. Ooi, S. Natarajan, A review of the scaled boundary finite element method for two-dimensional linear elastic fracture mechanics, Eng. Fract. Mech. 187 (2018) 45–73, http://dx.doi.org/10.1016/j.engfracmech.2017.10.016.

[26] T. Huang, J. Yang, J. Jin, P. Wen, M. Aliabadi, Evaluation of stress intensity factors and T-stress by finite block method: Static and dynamic, Theor. Appl. Fract. Mech. 93 (2018) 222–232, http://dx.doi.org/10.1016/j.tafmec.2017.08.009.

[27] H. Zhang, S. Liu, S. Han, L. Fan, Computation of T-stresses for multiple-branched and intersecting cracks with the numerical manifold method, Eng. Anal. Bound. Elem. 107 (2019) 149–158, http://dx.doi.org/10.1016/j.enganabound.2019.07.011.

[28] M. Aliabadi, Boundary element formulations in fracture mechanics, Appl. Mech. Rev. 50 (2) (1997) 83–96, http://dx.doi.org/10.1115/1.3101690.

[29] Y. Liu, S. Mukherjee, N. Nishimura, M. Schanz, W. Ye, A. Sutradhar, E. Pan, N. Dumont, A. Frangi, A. Saez, Recent advances and emerging applications of the boundary element method, Appl. Mech. Rev. 64 (3) (2011) http://dx.doi.org/10.1115/1.4005491.

[30] P. Olsen, Determining the stress intensity factors KI, KII and the T-term via the conservation laws using the boundary element method, Eng. Fract. Mech. 49 (1) (1994) 49–60, http://dx.doi.org/10.1016/0013-7944(94)90110-4.

[31] J. Sladek, V. Sladek, P. Fedelinski, Contour integrals for mixed-mode crack analysis: Effect of nonsingular terms, Theor. Appl. Fract. Mech. 27 (2) (1997) 115–127, http://dx.doi.org/10.1016/S0167-8442(97)00013-X.

[32] B. Yang, K. Ravi-Chandar, Evaluation of elastic T-stress by the stress difference method, Eng. Fract. Mech. 64 (5) (1999) 589–605, http://dx.doi.org/10.1016/s0013-7944(99)00082-x.

[33] C. Tan, X. Wang, The use of quarter-point crack-tip elements for T-stress determination in boundary element method analysis, Eng. Fract. Mech. 70 (15) (2003) 2247–2252, http://dx.doi.org/10.1016/S0013-7944(02)00251-5.

[34] J. Yu, C. Tan, X. Wang, T-stress solutions for cracks emanating from a circular hole in a finite plate, Int. J. Fract. 140 (1–4) (2006) 293–298, http://dx.doi.org/10.1007/s10704-006-0110-7.

[35] A. Sutradhar, G. Paulino, Symmetric Galerkin boundary element computation of T-stress and stress intensity factors for mixed-mode cracks by the interaction integral method, Eng. Anal. Bound. Elem. 28 (11) (2004) 1335–1350, http://dx.doi.org/10.1016/j.enganabound.2004.02.009.

[36] A.-V. Phan, A non-singular boundary integral formula for determining the T-stress for cracks of arbitrary geometry, Eng. Fract. Mech. 78 (11) (2011) 2273–2285, http://dx.doi.org/10.1016/j.engfracmech.2011.05.001.

[37] M. Chen, Z. Xu, X. Fan, Evaluation of the T-stress and stress intensity factor for multi-crack problem using spline fictitious boundary element alternating method, Eng. Anal. Bound. Elem. 94 (2018) 69–78, http://dx.doi.org/10.1016/j.enganabound.2018.06.004.

[38] W.-Z. Feng, L.-F. Gao, Y.-W. Dai, W. Qian, DBEM computation of T-stress and mixed-mode SIFs using interaction integral technique, Theor. Appl. Fract. Mech. 110 (2020) http://dx.doi.org/10.1016/j.tafmec.2020.102795.

[39] J. Yang, J. Liu, J. Sladek, V. Sladek, P. Wen, Stress intensity factors and T-stresses by boundary integral equations: 3D statics, Eng. Fract. Mech. 256 (2021) http://dx.doi.org/10.1016/j.engfracmech.2021.107917.

[40] P. Wen, J. Wen, J. Sladek, V. Sladek, Stress intensity factors and T-stresses for periodic array cracks: 3D static and dynamic, Theor. Appl. Fract. Mech. 117 (2022) http://dx.doi.org/10.1016/j.tafmec.2021.103198.

[41] H. Yu, M. Kuna, Interaction integral method for computation of crack parameters K – T – A review, Eng. Fract. Mech. 249 (2021) http://dx.doi.org/10.1016/j.engfracmech.2021.107722.

[42] A. Sáez, R. Gallego, J. Dominguez, Hypersingular quarter-point boundary elements for crack problems, Internat. J. Numer. Methods Engrg. 38 (10) (1995) 1681–1701, http://dx.doi.org/10.1002/nme.1620381006.

[43] F. García-Sánchez, A. Sáez, J. Domínguez, Anisotropic and piezoelectric materials fracture analysis by BEM, Comput. Struct. 83 (2005) 804–820, http://dx.doi.org/10.1016/j.compstruc.2004.09.010.

[44] F. García-Sánchez, A. Sáez, J. Domínguez, Two-dimensional time-harmonic BEM for cracked anisotropic solids, Eng. Anal. Bound. Elem. 30 (2) (2006) 88–99, http://dx.doi.org/10.1016/j.enganabound.2005.09.005.

[45] F. García-Sánchez, C. Zhang, A. Sáez, A two-dimensional time-domain boundary element method for dynamic crack problems in anisotropic solids, Eng. Fract. Mech. 75 (6) (2008) 1412–1430, http://dx.doi.org/10.1016/j.engfracmech.2007.07.021.

[46] R. Rojas-Díaz, F. García-Sánchez, A. Sáez, Analysis of cracked magnetoelectroelastic composites under time-harmonic loading, Int. J. Solids Struct. 47 (1) (2010) 71–80, http://dx.doi.org/10.1016/j.ijsolstr.2009.09.011.

[47] H.-K. Hong, J.-T. Chen, Derivations of integral equations of elasticity, J. Eng. Mech. 114 (6) (1988) 1028–1044, http://dx.doi.org/10.1061/(ASCE)0733-9399(1988)114:6(1028).

[48] A. Portela, M. Aliabadi, D. Rooke, The dual boundary element method: Effective implementation for crack problems, Internat. J. Numer. Methods Engrg. 33 (6) (1992) 1269–1287, http://dx.doi.org/10.1002/nme.1620330611.

[49] M. Aliabadi, The Boundary Element Method, Volume 2: Applications in Solids and Structures, John Wiley & Sons, Ltd., West Sussex, England, 2002, pp. 1–636.
[50] E. García-Macías, L. Rodríguez-Tembleque, A. Sáez, Mwcnt/epoxy strip-like sensors for buckling detection in beam-like structures, Thin-Walled Struct. 133 (2018) 27–41, http://dx.doi.org/10.1016/j.tws.2018.09.013.
[51] B. Karihaloo, Q. Xiao, X. Liu, Direct determination of SIF and coefficients of higher order terms of mixed mode cracks, Comput. Fluids Solid Mech. 125 (3–4) (2004) 207–225.
[52] D. Leonetti, S. Vantadori, Weight functions for stress intensity factor and T-stress derived for an inclined edge crack in a finite width plate, Int. J. Fatigue 165 (2022) http://dx.doi.org/10.1016/j.ijfatigue.2022.107170.
[53] B. Cotterell, J. Rice, Slightly curved or kinked cracks, Int. J. Fract. 16 (2) (1980) 155–169, http://dx.doi.org/10.1007/BF00012619.
[54] Y. Chen, Closed form solutions of T-stress in plane elasticity crack problems, Int. J. Solids Struct. 37 (11) (2000) 1629–1637, http://dx.doi.org/10.1016/S0020-7683(98)00312-6.